A comparison of fatigue strength sensitivity to defects for materials manufactured by AM or traditional processes

S. Beretta *, S. Romano

Politecnico di Milano, Department of Mechanical Engineering, Via La Masa 1, I-20156 Milan, Italy

Abstract

The fatigue behavior of metallic materials fabricated via additive manufacturing processes is currently not well understood and it has been the subject of many experimental investigations in recent years. In this paper we carried out a literature review about the fatigue strength of additively manufactured AlSi10Mg and Ti6Al4V, especially in terms of sensitivity to defects and inhomogeneities. The analysis shows that fatigue properties and key variables (heat treatment, defect size) are very similar to the ones of parts obtained with traditional manufacturing processes. These results confirm that defect tolerant design concepts can be adopted also for AM components.

Keywords:
Additive manufacturing AlSi10Mg
Ti-6Al-4V
Fatigue limit
DK_{th}
Short cracks

1. Introduction

The mechanical behavior and *fitness-for-purpose* of materials fabricated via additive manufacturing is currently not well understood and has been the subject of many experimental investigations in recent years. For instance, "because the ultimate mechanical behavior of metallic parts is related to their thermal-history-dependent microstructure, additive manufactured (AM) parts can have different, more anisotropic properties than wrought materials" (quote from [1]).

Regarding service life and durability, the fatigue properties of materials/components are usually controlled by the ineluctable presence of defects induced during the manufacturing process (casting, forging and AM processes) that significantly reduce the fatigue strength and overall life with respect to the theoretical properties of a given microstructure. This is because the presence of defects in a material means that the initial phases of fatigue damage that consist of the formation of slip-bands and micro-cracks, which are part of a process that occurs on an area the size of a few microstructural units, are bypassed [2,3]. A similar role is also played by the surface roughness of the material, which mod-ern studies have shown can be treated in the same way as short cracks [4,5].

From this point of view, the fatigue properties of materials fabricated using AM processes should not differ from those fabricated using traditional ones, except for the effects related to their *process-dependent* microstructure and typical features related to solidification of the *surface layers* in 3D-printed components [6,7].

The latter appears to be the first relevant issue for fatigue in AM materials because as-built parts exhibit a dramatic decrease in the fatigue performance, as much as 40–50% of that observed for the machined condition [8–11]. The high surface roughness acts as multiple stress concentrators. Tensile residual stresses, together with the presence of subsurface pores and defects [12], promote crack initiation (see Fig. 1 and the discussion in Section 5.2).

However, the same substantial reduction in fatigue strength is also observed for materials obtained using traditional processes, such as when the surface is very rough and characterized by fast solidification. As an example, EUROCODE 3 [13,14] reports a similar decrease in the fatigue properties for *machined thermally cut edges*. If we consider the *surface effects* associated with traditional plastic deformation processes (forging, drawing and roll milling), there are microfolds and oxides that become entrapped during the deformation of the surface layers. These can be analyzed by treating the defects as small cracks [15–17].

Therefore, it appears to be worthwhile to apply the methods developed for analyzing the fatigue strength of components obtained by *traditional* processes to AM. Such an approach was implemented on EBM Ti-Al alloys [18] and has proven to be a valuable tool, even for *microstructural inhomogeneities* [19].

The goal of this paper is to consider the fatigue strength of two materials, AlSi10Mg and Ti6Al4V, which are widely used in AM parts and to compare them with the properties obtained from

* Corresponding author.
E-mail address: stefano.beretta@polimi.it (S. Beretta).

Published Journal Article available at: http://dx.doi.org/10.1016/j.ijfatigue.2016.06.020

Nomenclature

AB	as-built (unmachined)
ALM	additive laser manufacturing
AM	additive manufacturing
CPUA/d_{grain}	cells per unit area/mean grain size
(S)DAS	(secondary) dendrite arm spacing
DMD	direct metal deposition
DMLS	direct metal laser sintering
EBM	electron beam melting
F_W	Murakami's geometric factor for estimating SIF
h/v	horizontal/vertical specimen axis orientation
HIP	hot isostatic pressing
HT	heat treatment
LENS	laser engineered net shaping
LEFM	linear elastic fracture mechanics
LP/HP	low/high laser source power
MA	milled annealed
n	slope of the $\sqrt{area} - \Delta K_{th}$ curve in a bi-logarithmic diagram
n'	slope of the $\sqrt{area} - \Delta\sigma_w$ curve in a bi-logarithmic diagram
HPDC	high pressure die casting
R	stress ratio ($\sigma_{min}/\sigma_{max}$)
SIF	stress intensity factor
SLM	selective laser melting
SMD	shape metal deposition
UTS	ultimate tensile strength
ΔK_{th}	crack propagation threshold
$\Delta K_{th,LC}$	crack propagation threshold for long cracks
$\Delta\sigma$	applied stress range
$\Delta\sigma_w$	fatigue limit
$\Delta\sigma_{w0}$	fatigue limit of the material without defects
σ_Y/YS	yield strength

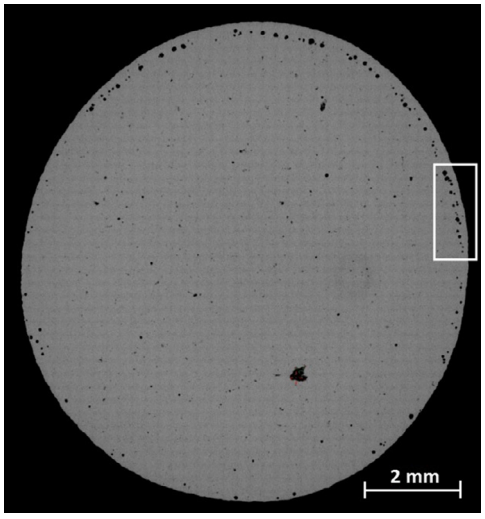

Fig. 1. CT scan of a 400 μm thick slice (inclined respect to the build direction) of an as-built part made of AlSi10Mg, where pores are present below the surface together with a significant volumetric defect (courtesy of RUAG Space (Zurich, CH)).

the same materials fabricated using traditional manufacturing processes in terms of the dependence of defect size and inhomogeneities. The analysis, which complements recent reviews [20], will show that the material properties in the presence of defects are quite similar for both additive and traditionally manufactured parts. This will allow us to discuss the prospective adoption of *defect-tolerant* design for the evaluation of the fitness for purpose of AM components.

2. Scope on fatigue strength in presence of defects

The estimation of fatigue strength and, especially, the quality control of components containing defects and inhomogeneities are very important problems. Complete solutions to these problems have only been determined in the mid-1980s. Experimental work by Murakami [21] has shown that small *non-propagating* cracks are always present at the tip of defects and micro-notches at stress levels near the fatigue limit and that the fatigue limit $\Delta\sigma_w$ is the threshold stress at which the small cracks do not propagate.

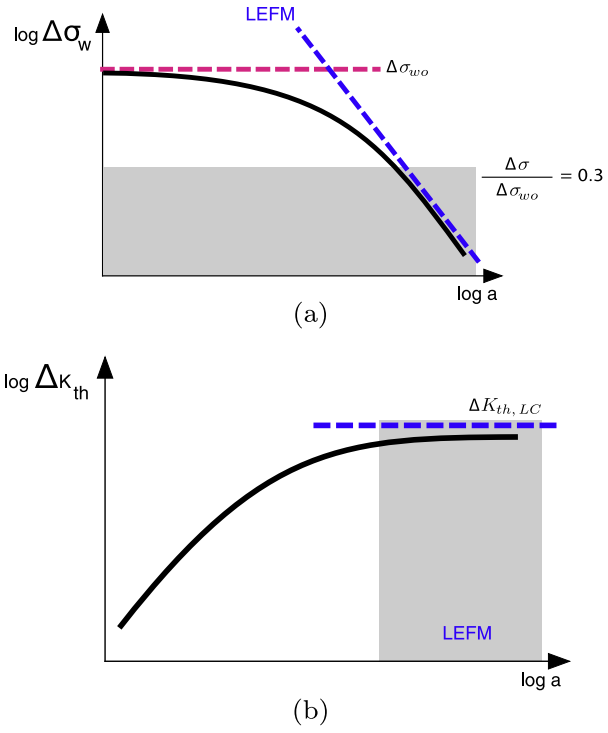

Fig. 2. Schematics of the typical trends for fatigue limit in presence of defects: (a) $\Delta\sigma_w$ vs. defect/crack; (b) dependence of ΔK_{th} on defect/crack size.

The typical features of the fatigue strength in presence of defects can be described by the so-called *Kitagawa-Takahashi* diagram [22], which is schematically depicted in Fig. 2. In terms of the fatigue limit, LEFM can be applied for predicting the fatigue strength for only low stress levels ($\sigma_w < 0.3 \cdot \sigma_Y$) or in the presence of large defects, whereas $\Delta\sigma_w$ increases when the defect/crack size decreases and $\Delta\sigma_w \rightarrow \Delta\sigma_{w0}$ when the crack size is very small. If the fatigue limit data are transformed into a prospective ΔK_{th} at the tip of small cracks (by using Eq. (1)), then the data show that $\Delta K_{th} \rightarrow \Delta K_{th,LC}$ only for very large defects/cracks. This justifies why LEFM cannot be adopted for predicting the fatigue strength with small defects.

Considering a crack with an irregular shape (or a defect with a small crack at its edge), the SIF range can be easily estimated using:

$$\Delta K = F_W \cdot \Delta S \cdot \sqrt{\pi \cdot \sqrt{area}} \quad (1)$$

where $\sqrt{area}$ is Murakami's parameter [23] for expressing the crack size, ΔS is the applied stress range and F_W depends on the crack location ($F_W = 0.65$ for surface cracks and $F_W = 0.5$ for internal cracks). Eq. (1), together with a suitable model for expressing the relationship between ΔK_{th} and crack size, allows the calculation of $\Delta\sigma_w$. According to Murakami & Endo [24], the threshold for small cracks can be expressed as:

$$\Delta K_{th} \propto \left(\sqrt{area}\right)^{1/3} \quad (2)$$

Combining Eq. (2) with Eq. (1) gives:

$$\Delta\sigma_w = \frac{C}{F_W \cdot \left(\sqrt{area}\right)^{1/6}} \quad (3)$$

where C is a parameter that depends on the material hardness and defect position. From Fig. 2b, using slope of the trend of ΔK_{th}, Eq. (2) can be generalized as $\Delta K_{th} \propto \left(\sqrt{area}\right)^{1/n}$, where $n = 2$ for very small cracks and $n \to \infty$ for long cracks. By adopting Eq. (1) the fatigue limit may be expressed as:

$$\Delta\sigma_w \propto \frac{1}{\left(\sqrt{area}\right)^{1/n'}} \quad (4)$$

where $n' = 1/(1/2 - 1/n)$ and $n' \geqslant 2$ ($n' = 2$ only for long cracks).

Another possibility for describing the Kitagawa diagram is to adopt the *El-Haddad model*. According to this model, if Eq. (1) is adopted for the SIF, the relationship between the fatigue limit and the defect/crack size can be expressed as:

$$\Delta\sigma_w = \Delta\sigma_{wo} \cdot \sqrt{\frac{\sqrt{area}_o}{\sqrt{area} + \sqrt{area}_o}} \quad (5)$$

and

$$\Delta K_{th} = \Delta K_{th,LC} \cdot \sqrt{\frac{\sqrt{area}}{\sqrt{area} + \sqrt{area}_o}} \quad (6)$$

where

$$\sqrt{area}_o = \frac{1}{\pi}\left(\frac{\Delta K_{th,LC}}{F_W \cdot \Delta\sigma_{wo}}\right)^2 \quad (7)$$

is called *El-Haddad parameter* (expressed with Murakami's $\sqrt{area}$ parameter). The advantage of these formulations is that they describe the smooth transition *short cracks* → *long cracks*, which corresponds to $n \to \infty$ for $\sqrt{area} > 10\sqrt{area}_o$ [25]. Other models can be applied for modeling the *Kitagawa diagram* (see the review in [26,27]).

3. Literature data on the fatigue properties for AM and comparison with traditional processes

In this section, we perform a literature review on AlSi10Mg and Ti6Al4V, which are very common alloys used in aerospace and lightweight design applications. The main goal of this section is to compare the literature data on the fatigue properties of parts obtained by AM with those from traditional manufacturing processes, a topic that was recently discussed by Li et al. [20] for Ti6Al4V. The focus is on the fatigue limit and the crack propagation threshold ΔK_{th} of the material collected for two different stress ratios ($R = 0.1$ and $R = -1$). The fatigue limit in the absence of defects and the crack propagation threshold are used to determine the left and right sides of the two prospective Kitagawa diagrams (shown in Fig. 2a and b). For references with detailed test results, the specimens that survived at least $5 \cdot 10^6$ cycles were considered for the fatigue limit determination. When the defect size was reported, a point was added to the Kitagawa diagrams. To increase the number of points, the prospective fatigue limit of the specimens that failed before $5 \cdot 10^6$ cycles was calculated by the slope of the S-N diagram of the same batch.

The AM results are depicted using red[1] marks and red dashed lines, whereas data pertaining to traditional manufacturing processes are shown in colored marks and gray regions. The same is done for the fatigue limit in the absence of defects (shown on the left hand side of Kitagawa diagram) and for the long crack propagation threshold $\Delta K_{th,LC}$ (shown on the right hand side of the Kitagawa diagram). The mean value for the AM data is depicted using red dashed lines, whereas the evidence for the standard processes is summarized by gray bands.

In most cases, the references do not specify whether the crack initiated from the surface or inside the specimen, thus increasing the scatter of the results. For the sake of the $\Delta K_{th} - \sqrt{area}$ diagram, the SIF was calculated using a factor $F_W = 0.65$ in Eq. (1) because most of the failures were triggered by surface defects. However, when the internal position is specified, a value of $F_W = 0.5$ was used.

3.1. AlSiMg alloys

Table 1 [6,8,28–32] and Table 2 [8,33–60] summarize the literature search results and, report the manufacturing process, the static and dynamic mechanical properties and the size of the dendrites, which are the microstructural features (whose direction and size depend on the cooling process) that most affect the fatigue resistance of the material [54,61]. The tables contain some other significant parameters, including (i) the mean grain size [33,34] (which is reported by some authors as CPUA), (ii) the effect of hot isostatic pressing [35] and (iii) the iron content [51]. The mechanical and fatigue properties, as well as the static resistance and yield stress, exhibit a large scatter between the references that appears to be due to *microstructure* and the heat treatment, which for this alloy is usually a T6 condition.

Among the analyzed documents, [6,8,28–32] report the fatigue limit of the specimens produced by SLM and consider different laser speeds, platform temperatures and specimen orientations with respect to the building direction. On some of the samples, a T6 heat treatment or HIP process was also performed.

Fig. 3 depicts the Kitagawa diagram for both $R = 0.1$ (Fig. 3a) and $R = -1$ (Fig. 3b). The influence of the dendrite size on $\Delta\sigma_{wo}$ is clearly visible [47,48,54].

Fig. 4 shows the Kitagawa diagram from another point of view: on the ordinate axis, the fatigue limit is replaced by the crack propagation threshold. The relation between (S) DAS and ΔK_{th} is reported by averaging the different literature results [40,42,58].

3.2. Ti6Al4V

The literature data for Ti6Al4V, which is a very common high strength alloy for aeronautics and space applications, are reported in Table 3 [8–11,62–78] and Table 4 [8,44,45,77,79–87].

There are a large number of publications relating to AM that are available for this material. Among these, several manufacturing techniques are analyzed. Most of these techniques utilize a powder bed, which is melted by a laser [8–10,62,63,67,68,76–78] or electron beam [11,68,69,78], whereas some others consider direct metal deposition in the form of wire [11,69,71]. Some of the documents propose the investigation of the properties of the as-built

[1] For interpretation of color in Fig. 2, the reader is referred to the web version of this article.

Table 1
Summary of bibliography for AlSi10Mg, additive manufacturing.

Ref	Process	UTS (MPa)	YS (MPa)	R	$\Delta\sigma_w$ (MPa)	ΔK_{th} (MPa $\sqrt{\text{m}}$)	(S) DAS (μm)	Notes
[6,28]	SLM	300–310	165–175	0.1	228			50 mm/s, h
	SLM	315–325	170–175	0.1	210			50 mm/s 45°
	SLM	225–230	100–105	0.1	165			50 mm/s, v
	SLM T6	330	275	0.1	145			50 mm/s, h
	SLM	325–375	245–255	0.1	140			500 mm/s, h
	SLM	295–320	255	0.1	100			500 mm/s 45°
	SLM	275–285	235–240	0.1	69			500 mm/s, v
	SLM T6	340–345	285–295	0.1	200			500 mm/s, h
	SLM T6	340–350	300–305	0.1	115			500 mm/s 45°
	SLM T6	325–335	290–285	0.1	140			500 mm/s, v
[29]	SLM	320–340		0.1	57			
	SLM HT	288–296		0.1	114			
[8]	SLM AB	358	227	−1	100			h
	SLM AB	289	172	−1	105			v
	SLM			−1	175			h
[30]	SLM			−1	210			BPH
[31]	SLM	357–366	198–205	−1	160			BPH, SR
[32]	SLM			−1	135			SR
	SLM			−1	185			BPH, SR

Table 2
Summary of bibliography for AlSi10Mg, traditional processes.

Ref	Process	UTS (MPa)	YS (MPa)	R	$\Delta\sigma_w$ (MPa)	ΔK_{th} (MPa $\sqrt{\text{m}}$)	(S) DAS (μm)	Notes
[33]	Cast T6	335	275	0.1	93–113		32–44	$d_{grain} = 550$ μm
[34]	Cast			0.1	126–132		30	$d_{grain} = 310$ μm
[35]	Cast	289–298	269–278	0.1	80			
	Cast	316–328	291–296	0.1	114–136			HIP
[36]	Cast			0.1	100–110	2.1–2.5		
[37,38]	Cast T6	260–265	236–245	0.1	100–120			
[39]	Cast			0.1		6.1	35–50	
[40]	Cast			0.1	100	3.5–5	20–25	
	Cast			0.1	70	5–6.5	70–75	
[41]	Cast T6	260	130	0.1		4		
[42]	Cast	267–276	224–231	0.1		6–6.2	80	
	Cast	255	218	0.1		6.9	90	
[43]	Inv. cast T6	331	272	0.1	146		47	
	Inv. cast T6	353	259	0.1	160		51	Sr
	Inv. cast T6	361	327	0.1	216		49	Sr-HIP
[44]	HPDC			0.1		3.3–3.7		
	HPDC			−1		6.1		
[45,46]	HPDC			0.1	62	3.8		
	HPDC			−1	100	6		
[47]	Cast T6	335	275	0.1	155		25–58	
	Cast T6	335	275	−1	100		25–58	
[48]	Cast T6			0.1	84–162		40–70	
	Cast T6			−1	114–180		40–70	
[49,50]	Sand cast	302	222	0	68–88		27–43	
	Sand cast	270	215	0	62–80		41–51	
				−1	76–96		27–43	
	Sand cast	295	228	−1	114–146		24–33	
	Sand cast			−1	114–146		33–44	
				−1	142–166		41–51	
[8]	wrought	310	293	−1	210			
[51]	Cast T6		220–270	−1	90–130			HIP low Fe
	Cast T6		220–270	−1	40–80			Low Fe
	Cast T6		220–270	−1	70–110			HIP high Fe
[52]	Sand cast T6	220	180	−1	160–220			
	Inv. cast T6	240	190	−1	160–220			
	PDC T6	240	140	−1	120–180			
[53]	Cast T6	310		−1	170–180			
[54]	Cast T6	270–300	230	−1	162–190		21–35	Sand
	Cast T6	300	245	−1	170–198		21–35	Perm. mould
[55]	Cast T6			−1	170–180			
[56,57]	Cast			−1	80–120			
[58]	Cast	223	160	−1	60	4.3	50	
	Cast	223	160	−1	60	3.6	25	
[59]	Cast T6	278–309	261–273	−1	170		22	
[60]	Cast T6	441	409	−1	140			

samples [67] and compare them after machining [8–10,77] and using different finishing processes [62].

The influences of heat treatment [68,71,76] and HIP [8,76,77] are also analyzed, as are those of shot-peening [10]. An important

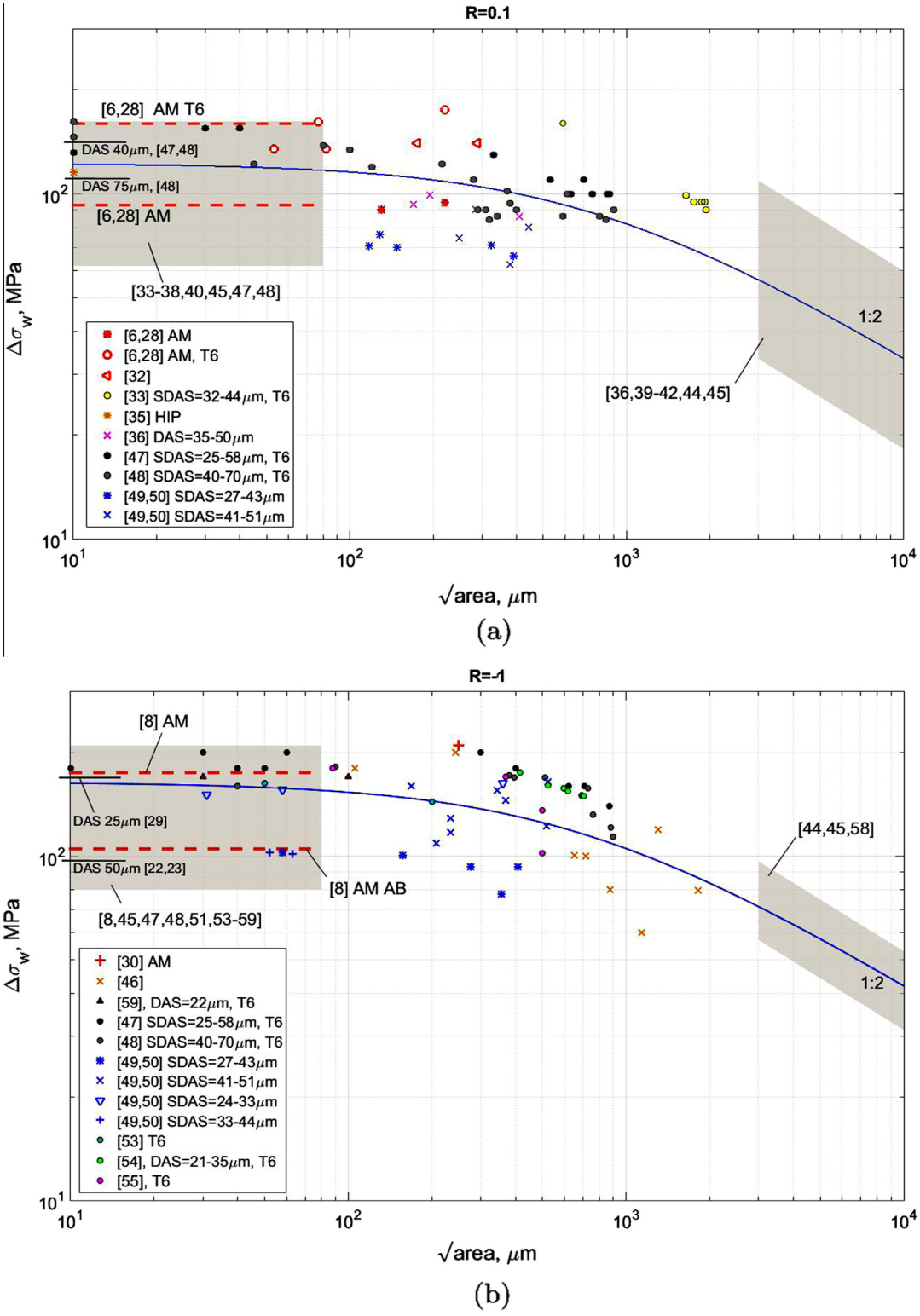

Fig. 3. Fatigue limit $\Delta\sigma_w$ of AlSi10Mg as a function of crack $\sqrt{area}$: (a) $R = 0.1$; (b) $R = -1$ (gray regions correspond to data for conventional processes).

difference in the crack propagation threshold is observed between the heat treated and the standard condition [76].

Eventually, the results from different additive manufacturing techniques are also presented: Zhai et al. [68] tested the endurance limit and crack propagation threshold of LENS before and after the heat treatment, using low and high laser powers and considering two specimen axis orientations. The same process is also tested in [63]. Baufeld et al. provided an overview of shape metal deposition and additive layer manufacturing and Greitemeier et al. [11,69,70] compared DMLS, EBM and DMD performed using laser or plasma arc.

Considering the results related to traditional processes, Léopold et al. [80] reported the fatigue limit of cast Ti6Al4V before and after machining. The influence that different microstructures have on

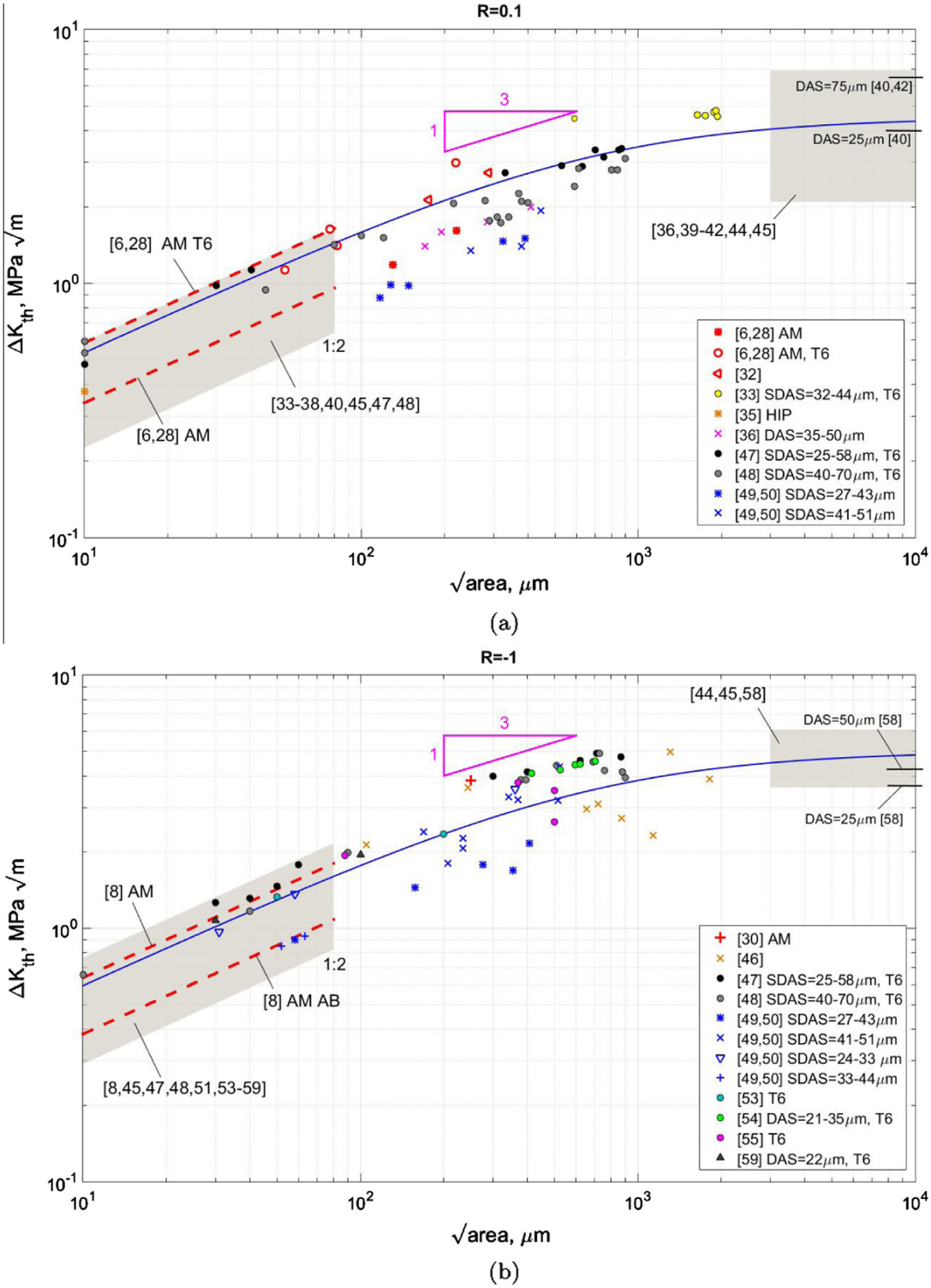

Fig. 4. Fatigue crack propagation threshold ΔK_{th} of AlSi10Mg as a function of crack $\sqrt{area}$: (a) $R = 0.1$; (b) $R = -1$ (gray regions correspond to data for conventional processes).

the dynamic properties is investigated in [44,81]. Most of the documents refer to forging processes in the milled-annealed condition or after heat treatment.

As described in Section 3.1, the Kitagawa diagram and the crack propagation threshold are depicted in Figs. 5 and 6. We also note that the defects reported by Giglio et al. [85] and Léopold et al.[80] are artificial and are created using electro discharge machin-ing. Artificial defects were also adopted by Gong et al. [67], who built defects directly during the 3D printing of the AM specimen.

4. Discussion

As seen in Figs. 3–6, the Kitagawa diagram provides a very good overview of the trend in the fatigue properties with respect to the defect size for both materials and is able to explain the large scatter for the different fatigue datasets. Moreover, the results from the AM processes are very similar to those for traditional manufacturing (casting, forging) and, sometimes, are even better.

Table 3
Summary of bibliography for Ti6Al4V, additive manufacturing.

Ref	Process	UTS (MPa)	YS (MPa)	R	$\Delta\sigma_w$ (MPa)	ΔK_{th} (MPa $\sqrt{\text{m}}$)	Notes
[9]	SLM	1140	1070	0.1	680–723	3.48	
[10]	SLM AB			0.1	210		
	SLM			0.1	510		
	SLM shot-peened			0.1	435		
[62]	LBM HIP, AB			0.1	158		
	LBM HIP, milling			0.1	540		
	LBM HIP, electr. pol.			0.1	450		
	LBM HIP, blasting			0.1	470		
[63]	LENS	1022	923	0.1	540		
[64,65]	EBM, AB			0.1		5.1–5.7	v
	EBM, AB			0.1		3.8	h
[66]	SLM	1240–1250	1100–1150	0.1	330–360		
	EBM	1010	950–960	0.1	540–600		
[67]	SLM AB			0.1	450		
[68]	LENS	1103	1005	0.1		2.87	LP h
	LENS HT	1073	1000	0.1		3.13	LP h
	LENS	1042	990	0.1		3.49	HP h
	LENS HT	1044	991	0.1		3.75	HP h
	LENS ann.	1030	970	0.1		4.81	h
	LENS	1103	1005	0.1		2.87	LP v
	LENS HT	1073	1000	0.1		3.68	LP v
	LENS	1042	990	0.1		3.19	HP v
	LENS HT	1044	991	0.1		3.88	HP v
	LENS ann.	1030	970	0.1		4.90	v
	EBM	1032–1066	973–1006	0.1		3.62	h
	EBM HT	1294	1039	0.1		3.81	h
	EBM	1073–1116	1001–1051	0.1		4.25	v
	EBM HT	1294	1039	0.1		5.45	v
[69]	DMLS HT	1170	1085	0.1	500	3–3.1	
	EBM HT	970 ± 10	870 ± 20	0.1	250	4–4.8	
	DMD-L HT	870	780 ± 20	0.1	540	5.3	
	DMD-P HT	810 ± 10	750 ± 25	0.1	450	5.3	
[11]	DMLS HT AB	1096 ± 7	1017 ± 7	0.1	180		
	EBM HT AB	965 ± 5	869 ± 7	0.1	135		
[70]	DMLS ann	1160–1170	1089–1103	0.1	500	3–3.2	
	DMLS HIP	993–1001	891–897	0.1	590	4.2–4.3	
	EBM ann	860–1084	849–887	0.1	240	4–4.6	
	EBM HIP	884–908	758–790	0.1	590	4.7–5	
[71]	SMD	1000	950	0.1	710–750		h
	SMD	950	900	0.1	685–730		v
	SMD HT	960–1000	930–960	0.1	700–720		h
	SMD HT	940–950	810–830	0.1	720–735		v
	ALM HT	980–1000	920–940	0.1	765–780		h
	ALM HT	890–970	900–880	0.1	700		v
[72]	SLM AB	1083–1259	1158–1287	0.1	550		
	EBM AB	908–984	855–909	0.1	340		
[73]	EBM AB	789–877	753–813	0.1		10	h
	EBM AB	813–889	788–836	0.1		9.2	v
[74]	SLM HT			0.1	400		BPH
[75]	EBM AB	1040–1085	940–1030	0.1	200–250		
	EBM AB	1060–1085	1020–1035	0.1	200–250		SR
	EBM HIP	1030	940–950	0.1	550–600		
[76]	SLM	1080 ± 30	1008 ± 30	0.1		1.4/1.7	h/v
	SLM HT 800 °C	1040 ± 30	962 ± 30	0.1		3.9 ± 0.4/4.6 ± 0.9	h/v
	SLM HT 1050 °C	945 ± 30	798 ± 30	0.1		3.9 ± 0.4/4.6 ± 0.9	h/v
	SLM HIP	1005 ± 30	912 ± 30	0.1		3.9 ± 0.4/4.6 ± 0.9	h/v
	SLM HT HIP			−1	605–635		
[8]	SLM HIP	950		−1	400		
	SLM AB HIP			−1	300		
[77]	SLM HIP	973–974	883–888	−1	500		
[78]	SLM HT			−1	760		BPH
	SLM HT HIP			−1	900		BPH
	EBM			−1	790		

The mean trend of the diagram can be well described using the El-Haddad formulation introduced in Eqs. (5) and (6) by considering a microstructural length of approximately 700 μm for AlSi10Mg and 200 μm for Ti6Al4V. The small amount of data in the literature on the size below which the defects are non-detrimental ([37,56] for AlSi10Mg and [10] for Ti6Al4V) are consistent with the Kitagawa diagrams in Figs. 3 and 5.

Regarding Murakami's model (Eq. (2)), Figs. 4 and 6 show the region of defect sizes where the slope of 1:3 describes the ΔK_{th} behavior. The range for this is 200 μm < $\sqrt{area}$ < 800 μm for the AlSi10Mg and 80 μm < $\sqrt{area}$ < 600 μm for Ti6Al4V. It is worth mentioning that the scatter along the ΔK_{th} diagram is lower than along $\Delta\sigma_w$ because of the precise calculation of the SIF using Eq. (1) for the different data points. Other results in the literature confirm the significant influence that defects have on AM parts.

According to Wycisk et al. [10], shot-peening does not improve the fatigue resistance when surface defects are eliminated. This is because cracks initiate from interior defects, where tensile stresses

Table 4
Summary of bibliography for Ti6Al4V, traditional processes.

Ref	Process	UTS (MPa)	YS (MPa)	R	$\Delta\sigma_w$ (MPa)	ΔK_{th} (MPa $\sqrt{m}$)	Notes
[79]	Wrought ann.	1000	924	0.1	410–520		
	Cast	1027	883	0.1	160–250		
[80]	Cast AB			0.1	150–270		
	Cast			0.1	230–380		
[81]	Forged HT	1055	975	0.1	515–540	5.7	Lamellar micr.
	Forged HT	978	930	0.1	450–540	4.3	Bimodal micr.
[82]	Forged MA	860–965	795–875	0	600–816		
	Cast	976	847	0	720		
	Formed	954	729	0	610–725		
[83]	Forged MA			0.1	620–640		
	Forged MA + overage			0.1	495–585		
[84]	Forged MA			0.1		10.37	
[44]	Forged			0.1		4.8–7	
	Forged			−1	450–600	9–13	
[45]	Forged MA			0.1		4.5–5.5	
	Forged			−1		7.5–10.1	
[85]	Forged			0.1		5.7	
	Forged			−1		9.8	
[86]	Forged			0.1	480–600		
	Forged			−1	774–846		
[8]	Wrought	1000		−1	630–680		
[77]	Wrought	973–1002	914–931	−1	600		
[87]	Wrought	1008–1012	917–623	−1	630		

induced by post-processing can have the opposite effect. Wycisk also acknowledges that the scatter associated with fatigue is related to defect size and location inside the specimen. This is as expected from Eq. (1); if defects are present in the sub-surface region, the fatigue limit is lower than if they are in a deeper position [9].

In addition to the common trend in the Kitagawa diagrams, which expresses a similar defect sensitivity for AlSi10Mg and Ti6Al4V manufactured by additive and traditional processes, it is worth re-considering the other factors that affect the fatigue properties of both materials.

4.1. Microstructure

The influence of the microstructure must be differentiated for the two materials. For AlSi10Mg, it is well known that the main variable affecting the fatigue limit in the left hand side of the Kitagawa diagram is the dendrite size, which controls the fatigue response [47,48,54]. This is also confirmed in [88,89], where the fatigue life was observed to be proportional to $DAS^{-1/2}$. Chen [90,91] reports that the fatigue life decreases six times in HCF and three times in LCF when DAS increases from 15 to 50 μm, as large DAS accelerates crack initiation. Similar trends are shown in Zang et al. [92]. For the additive processes, the fast cooling gra-dient associated with AM results in a very fine microstructure, which is very sensitive to the heat capacity data used and is char-acterized by columnar grains along the building direction and equiaxed grains in the cross section [93]. In the absence of large process-related defects, this microstructure is able to guarantee static properties and a hardness comparable and even higher than for a wrought material, even when heat treated [8,12], and can impede transgranular crack propagation.

However, for long crack propagation resistance, including fracture toughness and $\Delta K_{th,LC}$, a coarser microstructure favors crack deflection and energy dissipation at the crack tip and is responsible for increased resistance [40,42,58].

Considering Ti6Al4V, crack nucleation in absence of defects generally starts from equiaxed primary α phase or α lamellae [94]. Similar to AlSi10Mg, fatigue performance of smooth specimens increases when decreasing the α phase colony size (decreasing slip length) [20,81,94], whereas the crack propagation threshold decreases for a fine microstructure [11,44,69,94,95]. Note, however, that the crack orientation with respect to anisotropic microstructural features (e.g., columnar grains for AlSi10Mg or basket-weave and Widmanstätten for Ti6Al4V) can have an important effect on the nucleation and short crack propagation phases [96]. This is confirmed by [76], who showed a significant ΔK_{th} reduction when the crack path is perpendicular to the build direction.

4.2. As-built condition

The most evident issue is the effect of surface finishing. Unmachined parts exhibit a drastic decrease in the fatigue performance, as much as 40–50% with of the machined condition both for AlSi10Mg [8] and Ti6Al4V [9–11].

If a reduction of the fatigue limit is expected due to the presence of notches and residual stresses at the surface, the results by Leuders et al. [76] show also a significant decrease in $\Delta K_{th,LC}$ for the AB additively manufactured specimens. This result acknowledges the significant effect of *internal* residual stresses due to the additive processes (the different possibilities to avoid or eliminate internal residual stresses are discussed in the following section). Once again, this fact is in accordance with literature on welded structures.

Moreover, Fig. 5a suggests that the Kitagawa diagram vertically shifted to a lower value of $\Delta\sigma_w$ for AB parts. This is confirmed by the results from Greitemeier [11] who determined an *equivalent flaw size* (adopting LEFM), on the order of 200 μm, which is equivalent to the average $\sqrt{area}_o$ previously mentioned for Ti6Al4V.

4.3. Thermal treatment

A significant parameter affecting fatigue strength is the heat treatment after manufacturing.

For AlSi10Mg, the most common process is a peak hardening to the T6 condition, which ensures an improvement in the fatigue resistance of cast parts (comparing the data in [49,50] to [33,48] for $R = 0.1$ and to [52] for $R = -1$ in Table 2). The same effect is evident for AM components (Fig. 3a). Brandl et al. [6,28] recorded an increase in the fatigue limit after T6 hardening of 30–50% and

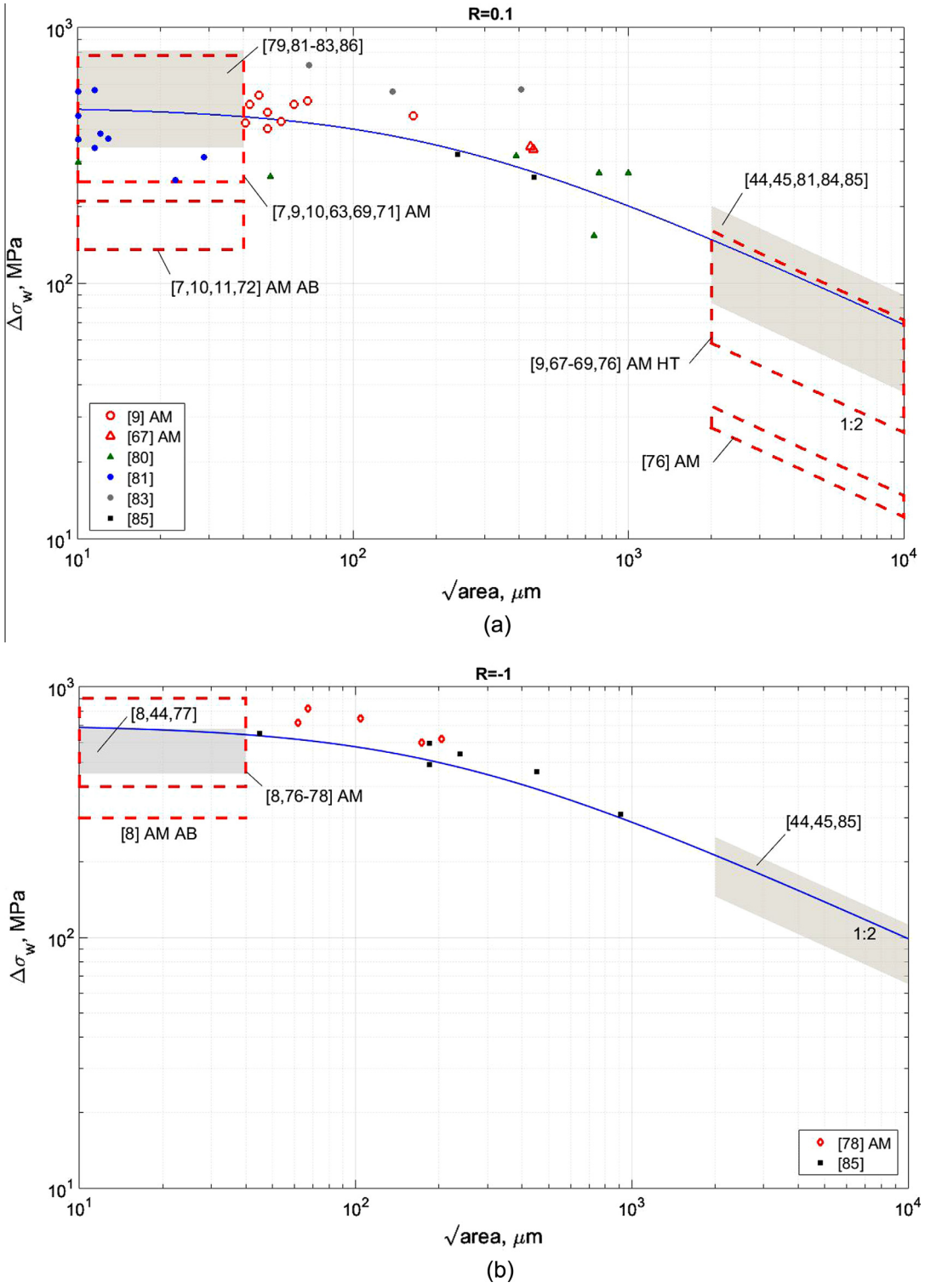

Fig. 5. Fatigue limit $\Delta\sigma_w$ of Ti6Al4V as a function of crack $\sqrt{area}$: (a) $R = 0.1$; (b) $R = -1$ (gray regions correspond to data for conventional processes).

reported that heat treatment eliminated dendrites (they became spherical), the heat affected zone and laser traces.

Considering Ti6Al4V, the thermal treatment can be different depending on the microstructure/mechanical properties that are desired in the final product. Wrought material is generally thermo-mechanically treated to $\alpha + \beta$ phase lamellae, together with some equiaxed α grains (known as a duplex alloy) [8,77]. Considering AM, the very fast cooling rate of SLM involves a very fine martensitic acicular α' microstructure (hcp), whereas for EBM the high process temperature provides in-process tempering of any martensite that forms due to the initial rapid cooling, resulting in a balanced $\alpha + \beta$ microstructure. This microstructure remains if annealing is performed at a temperature less than beta transus temperature (generally 600–700 °C) [9,77]. Higher than this temperature, the microstructure is composed of elongated α in a β matrix [68,77], which can also be obtained by HIP [76,77].

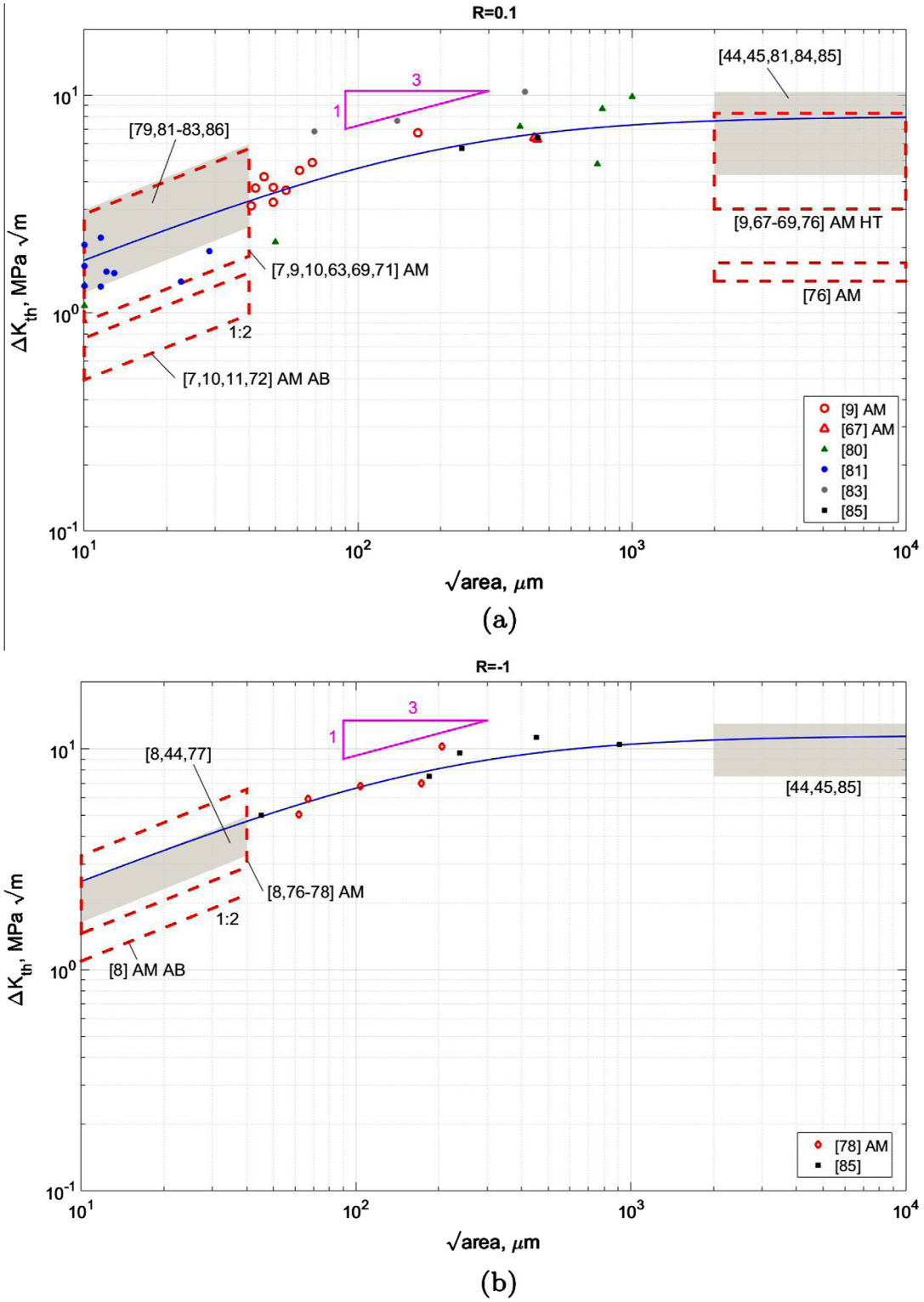

Fig. 6. Fatigue crack propagation threshold ΔK_{th} of Ti6Al4V as a function of crack $\sqrt{area}$: (a) $R = 0.1$; (b) $R = -1$ (gray regions correspond to data for conventional processes).

Whatever the HT, the conclusions that can be drawn for Ti6Al4V are similar to those for AlSi10Mg considering the improvement in the fatigue limit. In this case, a significant improvement in the crack propagation threshold is also highlighted [68,76]. The reason for this difference should be due to the presence of tensile residual stresses, which influence both ΔK_{th} and $\Delta\sigma_w$ over the entire defect size range.

Residual stresses after SLM can be removed by HT and HIP, paying attention not to coarsen the microstructure excessively [11]. Note that, as an additional effect, HIP closes internal porosity, thus providing a fatigue improvement moving to the left-hand side of the Kitagawa diagram. Another way to control porosity is to preheat the powder prior to melting every layer [6,76], which is always performed as a part of EBM. The importance of stress

relieving is highlighted by the results in [30–32] for SLM: a non-heat-treated specimen exhibited very high fatigue properties, even with respect to castings, just by pre-heating the powder to 200 °C.

5. Application of defect tolerance concepts

5.1. Fatigue strength for a given AM process

As described in the previous section, a single curve defining the general behavior of the material cannot be defined, although the scatter of the Ti6Al6V along the average Kitagawa diagram is relatively small. Thus, for instance, the $\sqrt{area}$ model from Murakami-Endo [24] can be applied to define the relationship between the $\Delta K_{th} - \sqrt{area}$. Alternatively, the precise properties for a given AM material can be determined by performing targeted fatigue tests with artificial micro-notches, which possess a larger $\sqrt{area}$ than the material defects, as was done in [18] for AM and in [17,60,85] for traditional processes.

Alternative methods are based on determining the *R-curve* from ΔK_{th} experiments and then the analytical calculation of the threshold stress for a crack emanating from a defect [97–100].

5.2. Equivalent defects for features of the as-built surface

A case study application is presented for a SLM component composed of AlSi10Mg and manufactured by RUAG (SLM process with platform pre-heating of 200 °C).

A series of CT scans on manufactured cylindrical specimens (the volume of the fatigue specimens is $V_S \approx 260$ mm^3) revealed internal volumetric defects with a size of 20 μm $< \sqrt{area} <$ 200 μm, which are mainly constituted by pores and lack of fusion between layers (one of these defects is visible in Fig. 1). Apart from volumetric defects, the real component is not machined and some regions exhibit sub-surface porosity (see Fig. 1), that (according to [101]) is typical for parts inclined respect to the build direction.

As discussed, surface effects are quite detrimental for the fatigue properties of unmachined components. However, if we adopt the concept that the Kitagawa diagram describes the fatigue properties of a component, then it would be worth calculating an *equivalent defect size* for the subsurface pores. Considering the schematic shown in Fig. 7a, it is clear that the subsurface pores (possessing a diameter of approx 80–100 μm and a maximum depth of 200–250 μm) can be approximated as 2D cracks with a depth t corresponding the defect depth. For this type of geometry, $\sqrt{area}$ can be calculated as [21]:

$$\sqrt{area} \simeq t \cdot \sqrt{10} \tag{8}$$

Considering a depth t of 200–250 μm, the equivalent $\sqrt{area}$ for the layer of sub-surface pores becomes $\sqrt{area}_{sub} = 630 - 790$ μm.

A series of HCF tests [30] on horizontal and vertical samples have been used to estimate the Kitagawa diagram at $R = -1$ (shown schematically in Fig. 7b). The histogram shows the size of the internal defects that are detected by CT scans, which have a mean dimensions of 50 μm.

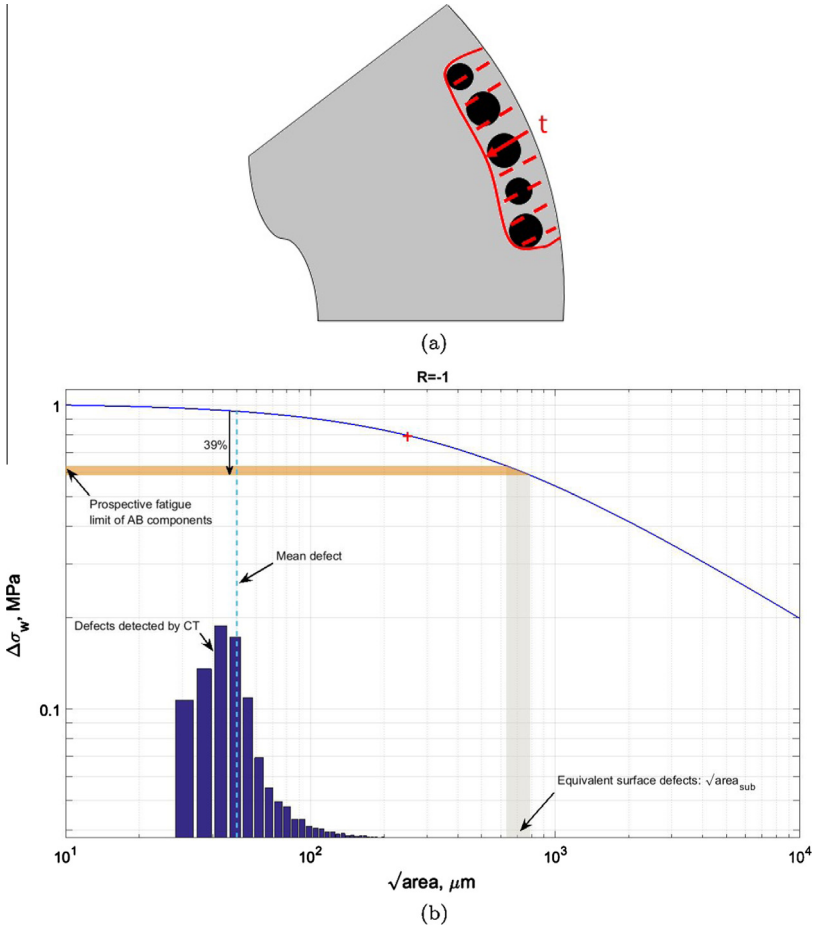

Fig. 7. Influence AB condition on the fatigue limit: (a) modelization of subsurface porosity as an equivalent surface crack; (b) reduction in the fatigue limit considering internal defects and equivalent surface defects from AB components (El-Haddad line calibrated on the data point reported in [30]).

The diagram clearly shows that the subsurface pores are much more detrimental than internal volumetric defects and it clearly depicts a *hierarchy* for the defects and inhomogeneities present in the component. In detail, the prospective reduction of fatigue strength with respect to the mean dimension of the small defects is approximately 39%, which is near to the 40% reported by Mower and Long [8] for AB specimens compared to machined samples.

5.3. Extreme defects and quality control

It is well known that for a given volume of material subjected to the same cyclic stress, fatigue failure or fracture will occur at the largest defect or inhomogeneity present in the volume. Therefore, the estimation of the fatigue strength in the presence of defects has been based on the prospective size of maximum defect in a given material volume (or batch of components) [102]. This analysis can be carried out adopting the concept of *statistics of extremes* [103,104]. A series of papers ([16,21] provide a summary of these studies) have shown the successful application of statistics of extremes for estimating the size of the maximum defect at the fracture origin or for expressing the *quality* of materials and components [105].

The fact that the sensitivity to the presence of defects can be described using the same methods adopted for materials/components manufactured using traditional processes opens the possibility of adopting the same *extreme value rating* concepts for quality control of AM materials/components. In this case, computed tomography scans are the standard control used for the identification of internal defects and the adoption of extreme value concepts is an interesting addition the to state-of-the-art for this topic [31,106,107]. In particular, extreme value concepts allow the determination of how the distribution of extreme defects increases with material volume and provides information on the minimum material volume that should be scanned for capturing the most detrimental defects [108].

6. Conclusions

In this paper we compared the fatigue strength of two materials, AlSi10Mg and Ti6Al4V, produced by AM and traditional manufacturing processes, in terms of the dependence on the size of defects and inhomogeneities. The significant results from this analysis are as follows:

- The wide scatter of the fatigue properties for machined AM materials is significantly reduced if the data are correlated to the defect size at the failure origin and depict the typical *Kitagawa-Takahashi* diagram.
- Fatigue strength of AlSi10Mg and Ti6Al4V obtained by AM are similar and sometimes better with respect to the properties of the same materials manufactured by traditional processes (casting, forging, etc.) if the test pieces have been machined and stress relieved.
- The fatigue strength of both materials at stress ratios of $R = 0.1$ and $R = -1$ can be averagely described in terms of the El-Haddad model, respectively assuming that $\sqrt{area}_o = 700\ \mu m$ and $\sqrt{area}_o = 200\ \mu m$.
- The crack propagation thresholds for small cracks/defects after heat treatment or HIP exhibit a significant increase with respect to the AB condition, for the fatigue strength for both materials.

These results support the adoption of *defect-tolerant design* and *extreme value defect ratings* that have been developed for analyzing correlations between the fatigue strength and manufacturing processes.

Acknowledgements

We would like to thank ESA staff, especially Ana Brandão for careful CT scans of volumetric defects, and Dr. T. Ghidini and J. Gumpinger for permission to publish results (CT scan measurements and fatigue data). We acknowledge permission by Ruag Space (Zurich, CH) to publish pictures of a CT scan, together with permission to publish CT scan data.

References

[1] Thompson SM, Bian L, Shamsaei N, Yadollahia A. An overview of Direct Laser Deposition for additive manufacturing; Part I: transport phenomena, modeling and diagnostics. Addit Manuf 2015;8:36–62.

[2] Miller K. The short crack problem. Fatigue Fract Eng Mater Struct 1982;5 (3):223–32.

[3] Schijve J. Fatigue of structures and materials. Dordrecht: Kluwer Academic Publishers; 2001.

[4] Takahashi K, Murakami Y. Quantitative evaluation of effect of surface roughness on fatigue strength. In: Benyon J, Brown M, Smith R, Lindley T, Tomkins B, editors. Engineering against fatigue. Balkema Publishers; 1999.

[5] Suraratchai M, Limido J, Mabru C, Chieragatti R. Modelling the influence of machined surface roughness on the fatigue life of aluminium alloy. Int J Fatigue 2008;30(12):2119–26.

[6] Brandl E, Heckenberger U, Holzinger V, Buchbinder D. Additive manufactured AlSi10Mg samples using selective laser melting (SLM): microstructure, high cycle fatigue, and fracture behavior. Mater Des 2012;34:159–69. http://dx.doi.org/10.1016/j.matdes.2011.07.067.

[7] Bagehorn S, Mertens T, Greitemeyer D, Carton L, Schoberth A. Surface finishing of additive manufactured Ti-6Al-4V – a comparison of electrochemical and mechanical treatments. In: 6th Eur conf aerosp sci; 2015.

[8] Mower TM, Long MJ. Mechanical behavior of additive manufactured, powder-bed laser-fused materials. Mater Sci Eng A 2015;651:198–213. http://dx.doi.org/10.1016/j.msea.2015.10.068.

[9] Wycisk E, Solbach A, Siddique S, Herzog D, Walther F, Emmelmann C. Effects of defects in laser additive manufactured Ti-6Al-4V on fatigue properties. Phys Procedia 2014;56:371–8. http://dx.doi.org/10.1016/j.phpro.2014.08.120.

[10] Wycisk E, Emmelmann C, Siddique S, Walther F. High cycle fatigue (HCF) performance of Ti-6Al-4V alloy processed by selective laser melting. Adv Mater Res 2013;816–817(September):134–9. http://dx.doi.org/10.4028/www.scientific.net/AMR.816-817.134.

[11] Greitemeier D, Dalle Donne C, Syassen F, Eufinger J, Melz T. Effect of surface roughness on fatigue performance of additive manufactured Ti-6Al-4V. Mater Sci Technol http://dx.doi.org/10.1179/1743284715Y.0000000053.

[12] Kempen K, Thijs L, Van Humbeeck J, Kruth JP. Mechanical properties of AlSi10Mg produced by selective laser melting. Phys Procedia 2012;39:439–46. http://dx.doi.org/10.1016/j.phpro.2012.10.059.

[13] ISO EN 1993. Eurocode 3: design of steel structures. ISO; 2005.

[14] Hobbacher A. Recommendations for fatigue design of welded joints and components. IIW document XIII-2151-07/XV-1254-07; 2007.

[15] Beretta S. Defect tolerant design of automotive components. Int J Fatigue 1997;4(19):319–33.

[16] Murakami Y, Beretta S. Small defects and inhomogeneities in fatigue strength: experiments, models and statistical implications. Extremes 1999;2(2):123–47.

[17] Cristea M, Beretta S, Altamura A. Fatigue limit assessment on seamless tubes in presence of inhomogeneities: small crack model vs. full scale testing experiments. Int J Fatigue 2012;41:150–7.

[18] Filippini M, Beretta S, Patriarca L, Pasquero G, Sabbadini S. Fatigue sensitivity to small defects of a gamma–titanium–aluminide alloy. Fatigue fracture mechanics, vol. 38. ASTM International; 2012.

[19] Beretta S, Filippini M, Patriarca L, Sabbadini S. Analysis of fatigue damage accumulation in TiAl intermetallics. Key engineering materials, vol. 592. Trans Tech Publ; 2014. p. 30–5.

[20] Li P, Warner D, Fatemi A, Phan N. Critical assessment of the fatigue performance of additively manufactured Ti–6Al–4V and perspective for future research. Int J Fatigue 2016;85:130–43.

[21] Murakami Y. Metal fatigue: effects of small defects and nonmetallic inclusions. Oxford: Elsevier; 2002.

[22] Kitagawa H, Takahashi S. Applicability of fracture mechanics to very small cracks or the cracks in the early stage. In: Proc 2nd int conf mech behaviour of materials – ICM2. p. 627–31.

[23] Murakami Y. Analysis of stress intensity factor of modes I, II and III for inclined surface cracks of arbitrary shape. Eng Fract Mech 1985;22:101–14.

[24] Murakami Y, Endo M. Effect of hardness and crack geometries on ΔK_{th} of small cracks emanating from small defects. In: Miller K, Rios EDL, editors. The behaviour of short fatigue cracks. MEP; 1986.

[25] Suresh S, Ritchie RO. Propagation of short fatigue cracks. Int Met Rev 1984;29 (6):445–76. http://dx.doi.org/10.1179/imtr.1984.29.1.445.

[26] Murakami Y, Endo M. Effect of defects, inclusions and inhomogeneities on fatigue strength. Int J Fatigue 1994;16:163–82.

[27] Zerbst U, Vormwald M, Pippan R, Gänser H-P, Sarrazin-Baudoux C, Madia M. About the fatigue crack propagation threshold of metals as a design criterion–a review. Eng Fract Mech 2016;153:190–243.

[28] Buchbinder D, Meiners W. Generative Fertigung von Aluminiumbauteilen für die Serienproduktion. Tech rep. Fraunhofer Institute; 2011.

[29] Maskery I, Aboulkhair NT, Tuck C, Wildman RD, Ashcroft IA, Everitt NM, et al. Fatigue performance enhancement of selectively laser melted aluminium alloy by heat treatment. Solid Free Fabr Symp 2015:1017–25.

[30] Brandão A, Gerard R, Gumpinger J, Ghidini T. X-ray CT and fatigue investigations on additive manufactured materials. In: Techinical interchang meet. Noordwijk, NL: ESTEC; 2015.

[31] Siddique S, Imran M, Rauer M, Kaloudis M, Wycisk E, Emmelmann C, et al. Computed tomography for characterization of fatigue performance of selective laser melted parts. Mater Des 2015;83:661–9. http://dx.doi.org/10.1016/j.matdes.2015.06.063.

[32] Siddique S, Imran M, Walther F. Very high cycle fatigue and fatigue crack propagation behavior of selective laser melted AlSi12 alloy. Int J Fatigue 2016;94:246–54. http://dx.doi.org/10.1016/j.ijfatigue.2016.06.003.

[33] Serrano-Munoz I, Buffiere J-Y, Verdu C, Gaillard Y, Mu P, Nadot Y. Influence of surface and internal casting defects on the fatigue behaviour of A357-T6 cast aluminium alloy. Int J Fatigue 2016;82:361–70. http://dx.doi.org/10.1016/j.ijfatigue.2015.07.032.

[34] Buffière JY, Savelli S, Jouneau PH, Maire E, Fougères R. Experimental study of porosity and its relation to fatigue mechanisms of model Al-Si7-Mg0.3 cast Al alloys. Mater Sci Eng A 2001;316(1–2):115–26. http://dx.doi.org/10.1016/S0921-5093(01)01225-4.

[35] Lee MH, Kim JJ, Kim KH, Kim NJ, Lee S, Lee EW. Effects of HIPping on high-cycle fatigue properties of investment cast A356 aluminum alloys. Mater Sci Eng A 2003;340(1–2):123–9. http://dx.doi.org/10.1016/S0921-5093(02)00157-0.

[36] Casellas D, Pérez R, Prado JM. Fatigue variability in Al-Si cast alloys. Mater Sci Eng A 2005;398(1–2):171–9. http://dx.doi.org/10.1016/j.msea.2005.03.034.

[37] Wang QG, Apelian D, Lados DA. Fatigue behavior of A356/357 aluminum cast alloys. Part II. Effect of microstructural constituents. J Light Met 2001;1:85–97. http://dx.doi.org/10.1016/S1471-5317(00)00009-2.

[38] Wang QG, Apelian D, Lados DA. Fatigue behavior of A356-T6 aluminum cast alloys. Part I. Effect of casting defects. J Light Met 2001;1(1):73–84. http://dx.doi.org/10.1016/S1471-5317(00)00008-0.

[39] Hertzberg RW. Deformation and fracture mechanics of engineering materials. 4th ed, 1996. http://dx.doi.org/10.1016/0261-3069(84)90070-0.

[40] Lados DA. Fatigue crack growth mechanisms in Al-Si-Mg alloys Doctoral thesis. Worchester Polytechnic Institute; 2004.

[41] Skallerud B, Iveland T, Härkegård G. Fatigue life assessment of aluminum alloys with casting defects. Eng Fract Mech 1993;44(6):857–74. http://dx.doi.org/10.1016/0013-7944(93)90108-5.

[42] Wigant C, Stephens R. Fatigue crack growth behaviour of A356-T6 aluminium alloy. Proc int conf fatigue, vol. 87. p. 165–73.

[43] Dezecot S, Brochu M. Microstructural characterization and high cycle fatigue behavior of investment cast A357 aluminum alloy. Int J Fatigue 2015;77:154–9. http://dx.doi.org/10.1016/j.ijfatigue.2015.03.004.

[44] Oberwinkler B, Riedler M, Eichlseder W. Importance of local microstructure for damage tolerant light weight design of Ti-6Al-4V forgings. Int J Fatigue 2010;32(5):808–14. http://dx.doi.org/10.1016/j.ijfatigue.2009.06.021.

[45] Oberwinkler B,Redik S, Leitner H. Analysis of short crack growth for two representative light metals. In: ICF12; 2009. p. 1–9.

[46] Oberwinkler C, Leitner H, Eichlseder W. Computation of fatigue safety factors for high-pressure die cast (HPDC) aluminum components taking into account the pore size distribution international.

[47] Mu P, Nadot Y, Mendez J, Ranganathan N. Influence of casting defects on the fatigue limit of nodular cast iron. Int J Fatigue 2004;26(3):311–9. http://dx.doi.org/10.1016/S0142-1123(03)00141-5.

[48] Houria MI, Nadot Y, Fathallah R, Roy M, Maijer DM. Influence of casting defect and SDAS on the multiaxial fatigue behaviour of A356-T6 alloy including mean stress effect. Int J Fatigue 2015;80:90–102. http://dx.doi.org/10.1016/j.ijfatigue.2015.05.012.

[49] Beretta S, Clerici P. Stima della resitenza a fatica in getti di AlSi7Mg. In: Atti della Giorn. di Stud. La fatica nelle leghe di Allum. Padova: AIM; 1997.

[50] Beretta S. Fatigue strength assessment of AlSi7Mg castings. In: Proc an int conf importance underst fundam fatigue process counteracting its eff eng components struct to reflect contrib K.J. Mill. Sheffield, Un. Rotterdam: Balkema Publishers; 1999.

[51] Gao YX, Yi JZ, Lee PD, Lindley TC. A micro-cell model of the effect of microstructure and defects on fatigue resistance in cast aluminum alloys. Acta Mater 2004;52(19):5435–49. http://dx.doi.org/10.1016/j.actamat.2004.07.035.

[52] UNI EN 1706. Alluminio e leghe di alluminio - Getti - Composizione chimica e proprietà meccaniche; 2010.

[53] McDowell DL, Gall K, Horstemeyer MF, Fan J. Microstructure-based fatigue modeling of cast A356-T6 alloy. Eng Fract Mech 2003;70(1):49–80. http://dx.doi.org/10.1016/S0013-7944(02)00021-8.

[54] Linder J, Axelsson M, Nilsson H. The influence of porosity on the fatigue life for sand and permanent mould cast aluminium. Int J Fatigue 2006;28 (12):1752–8. http://dx.doi.org/10.1016/j.ijfatigue.2006.01.001.

[55] Roy M, Nadot Y, Maijer DM, Benoit G. Multiaxial fatigue behaviour of A356-T6. Fatigue Fract Eng Mater Struct 2012;35(12):1148–59. http://dx.doi.org/10.1111/j.1460-2695.2012.01702.x.

[56] Ødegård J, Pedersen K. Fatigue properties of an A356 (AlSi7Mg) aluminium alloy for automotive applications - fatigue life prediction; 1994. http://dx.doi.org/10.4271/940811.

[57] Yi JZ, Gao YX, Lee PD, Lindley TC. Effect of Fe-content on fatigue crack initiation and propagation in a cast aluminum-silicon alloy (A356-T6). Mater Sci Eng A 2004;386(1–2):396–407. http://dx.doi.org/10.1016/j.msea.2004.07.044.

[58] Stanzl-Tschegg S. Fatigue and fatigue crack propagation in AlSi7Mg cast alloys under in-service loading conditions. Int J Fatigue 1995;17(2):149–55. http://dx.doi.org/10.1016/0142-1123(95)95895-N.

[59] Ceschini L, Morri A, Sambogna G. The effect of hot isostatic pressing on the fatigue behaviour of sand-cast A356-T6 and A204-T6 aluminum alloys. J Mater Process Technol 2008;204(1–3):231–8. http://dx.doi.org/10.1016/j.jmatprotec.2007.11.067.

[60] Kobayashi H, Ikeda H, Murakami Y. Extra-long life fatigue properties of Al-Si eutectic alloy by rotating bending and tension-compression fatigue tests. Trans Jpn Soc Mech Eng Ser A 1996;62(594):347–55.

[61] Major JF. Porosity control and fatigue behavior in A356-T61 aluminum alloy. AFS Trans 2002:901–6.

[62] Bagehorn S, Mertens T, Greitemeier D, Carton L, Schoberth A. Surface finishing of additive manufactured Ti-6Al-4V – a comparison of electrochemical and mechanical treatments. In: 6th Eur conf aerosp sci.

[63] Grylls R. LENS process white paper: fatigue testing of LENS Ti-6-4. Tech rep. Optomec; 2005.

[64] Seifi M, Dahar M, Aman R, Harrysson O, Beuth J, Lewandowski JJ. Evaluation of orientation dependence of fracture toughness and fatigue crack propagation behavior of as-deposited ARCAM EBM Ti-6Al-4V. JOM J Miner Met Mater Soc 2015;67(3):597–607. http://dx.doi.org/10.1007/s11837-015-1298-7.

[65] Seifi M, Salem A, Satko D, Shaffer J, Lewandowski JJ. Defect distribution and microstructure heterogeneity effects on fracture resistance and fatigue behavior of EBM Ti–6Al–4V. Int J Fatigue 2016;94:263–87. http://dx.doi.org/10.1016/j.ijfatigue.2016.06.001.

[66] Gong H, Rafi K, Gu H, Janaki Ram GD, Starr T, Stucker B. Influence of defects on mechanical properties of Ti-6Al-4V components produced by selective laser melting and electron beam melting. Mater Des 2015;86:545–54. http://dx.doi.org/10.1016/j.matdes.2015.07.147.

[67] Gong H, Rafi HK, Starr TL, Stucker BE. Effect of defects on fatigue tests of as-built Ti-6Al-4V parts fabricated by selective laser melting. In: Proc solid free fabr symp; 2012. p. 499–506.

[68] Zhai Y, Galarraga H, Lados DA. Microstructure evolution, tensile properties, and fatigue damage mechanisms in Ti-6Al-4V alloys fabricated by two additive manufacturing techniques. Procedia Eng 2015;114:658–66. http://dx.doi.org/10.1016/j.proeng.2015.08.007.

[69] Greitemeier D, Dalle Donne C, Schoberth A, Jürgens M, Eufinger J, Melz T, et al. Microstructure and mechanical properties. Appl Mech Mater 2015;807:169–80. http://dx.doi.org/10.4028/www.scientific.net/AMM.807.169.

[70] Greitemeier D, Palm F, Syassen F, Melz T. Fatigue performance of additive manufactured TiAl6V4 using electron and laser beam melting. Int J Fatigue 2016:1–7. http://dx.doi.org/10.1016/j.ijfatigue.2016.05.001.

[71] Baufeld B, Brandl E, Van Der Biest O. Wire based additive layer manufacturing: comparison of microstructure and mechanical properties of Ti-6Al-4V components fabricated by laser-beam deposition and shaped metal deposition. J Mater Process Technol 2011;211(6):1146–58. http://dx.doi.org/10.1016/j.jmatprotec.2011.01.018.

[72] Rafi HK, Karthik NV, Gong H, Starr TL, Stucker BE. Microstructures and mechanical properties of Ti6Al4V parts fabricated by selective laser melting and electron beam melting. J Mater Eng Perform 2013;22(12):3872–83. http://dx.doi.org/10.1007/s11665-013-0658-0.

[73] Edwards P, O'Conner A, Ramulu M. Electron beam additive manufacturing of titanium components: properties and performance. J Manuf Sci Eng 2013;135 (6):061016. http://dx.doi.org/10.1115/1.4025773.

[74] Xu W, Sun S, Elambasseril J, Liu Q, Brandt M, Qian M. Ti-6Al-4V additively manufactured by selective laser melting with superior mechanical properties. JOM 2015;67(3):668–73. http://dx.doi.org/10.1007/s11837-015-1297-8.

[75] Hrabe N, Gnäupel-Herold T, Quinn T. Fatigue properties of a titanium alloy (Ti-6Al-4V) fabricated via electron beam melting (EBM): effects of internal defects and residual stress. Int J Fatigue 2016;94:202–10. http://dx.doi.org/10.1016/j.ijfatigue.2016.04.022.

[76] Leuders S, Thöne M, Riemer A, Niendorf T, Tröster T, Richard HA, et al. On the mechanical behaviour of titanium alloy TiAl6V4 manufactured by selective laser melting: fatigue resistance and crack growth performance. Int J Fatigue 2013;48:300–7. http://dx.doi.org/10.1016/j.ijfatigue.2012.11.011.

[77] Kasperovich G, Hausmann J. Improvement of fatigue resistance and ductility of TiAl6V4 processed by selective laser melting. J Mater Process Technol 2015;220:202–14. http://dx.doi.org/10.1016/j.jmatprotec.2015.01.025.

[78] Günther J, Krewerth D, Lippmann T, Leuders S, Tröster T, Weidner A. Fatigue life of additively manufactured Ti-6Al-4V in the very high cycle fatigue regime. Int J Fatigue 2016;94:236–45. http://dx.doi.org/10.1016/j.ijfatigue.2016.05.018.

[79] Military Handbook. Titanium and titanium alloys, no. June. Washington D.C.: Department of Defense; 1974.

[80] Léopold G, Nadot Y, Billaudeau T, Mendez J. Influence of artificial and casting defects on fatigue strength of moulded components in Ti-6Al-4V alloy. Fatigue Fract Eng Mater Struct 2015;38(9):1026–41. http://dx.doi.org/10.1111/ffe.12326.

[81] Nalla RK, Boyce BL, Campbell JP, Peters JO, Ritchie RO. Influence of microstructure on high-cycle fatigue of Ti-6Al-4V: bimodal vs. lamellar structures. Metall Mater Trans A 2002;33(13):899–918. http://dx.doi.org/10.1007/s11661-002-1023-3.
[82] Niinomi M. Mechanical properties of biomedical titanium alloys. Mater Sci Eng A 1998;243(1–2):231–6. http://dx.doi.org/10.1016/S0921-5093(97)00806-X.
[83] Oguma H, Nakamura T. The effect of microstructure on very high cycle fatigue properties in Ti-6Al-4V. Scr Mater 2010;63(1):32–4. http://dx.doi.org/10.1016/j.scriptamat.2010.02.043.
[84] Nakamura T, Oguma H, Shinohara Y. Procedia engineering the effect of vacuum-like environment inside sub-surface fatigue crack on the formation of ODA fracture surface in high strength steel. Procedia Eng 2010;2 (1):2121–9. http://dx.doi.org/10.1016/j.proeng.2010.03.228.
[85] Giglio M, Beretta S, Mariani U, Ratti G. Defect tolerance assessment of a helicopter component subjected to multiaxial load. Eng Fract Mech 2010;77 (13):2479–90. http://dx.doi.org/10.1016/j.engfracmech.2010.06.012.
[86] Morrissey R, Nicholas T. Staircase testing of a titanium alloy in the gigacycle regime. Int J Fatigue 2006;28(11):1577–82. http://dx.doi.org/10.1016/j.ijfatigue.2005.10.007.
[87] Heinz S, Eifler D. Crack initiation mechanisms of Ti6Al4V in the very high cycle fatigue regime. Int J Fatigue 2016:4–11. http://dx.doi.org/10.1016/j.ijfatigue.2016.04.026.
[88] Wickberg A, Gustafsson G, Larsson L. Microstructural effects on the fatigue properties of a cast Al7SiMg alloy; 1984. http://dx.doi.org/10.4271/840121.
[89] Allison J, Jones J, Caton M, Boileau J. Microstructural influences on the fatigue of cast aluminum. In: Fatigue'99 – proc 7th int fatigue conf.
[90] Chen W, Zhang B, Wu T, Poirier D, Sung P, Fang QT. Microstructure dependence of fatigue life for A356.2. In: TMS annu meet, minerals, metals & materials soc (TMS); 1998. p. 99–113.
[91] Chen W, Zhang B, Wu T, Poirier D, Sung P, Fang Q. The role of dendrite arm spacing in fatigue of aluminium castings. In: 1st int Al cast tech symp, Rosemont, Ill; 1998.
[92] Zhang B, Chen W, Poirier D. Effect of solidification cooling rate on the fatigue life of A356.2-T6 cast aluminium alloy. Fatigue Fract Eng Mater Struct 2000;23(5):417–23. http://dx.doi.org/10.1046/j.1460-2695.2000.00299.x.
[93] Tradowsky U, White J, Ward RM, Read N, Reimers W, Attallah MM. Selective laser melting of AlSi10Mg: influence of post-processing on the microstructural and tensile properties development. Mater Des 2016;105:212–22. http://dx.doi.org/10.1016/j.matdes.2016.05.066.
[94] Polasik A. The role of microstructure on high cycle fatigue lifetime variability in Ti-6Al-4V Doctoral thesis. The Ohio State University; 2014.
[95] Lütjering G. Influence of processing on microstructure and mechanical properties of ($\alpha + \beta$) titanium alloys. Mater Sci Eng A 1998;243(1–2):32–45. http://dx.doi.org/10.1016/S0921-5093(97)00778-8.
[96] Collins PC, Brice D, Samimi P, Ghamarian I, Fraser H. Microstructural control of additively manufactured metallic materials. Annu Rev Mater Res 2016;46 (1). http://dx.doi.org/10.1146/annurev-matsci-070115-031816.
[97] Zerbst U, Madia M, Beier HT. A model for fracture mechanics based prediction of the fatigue strength: further validation and limitations. Eng Fract Mech 2014;130:65–74.
[98] Maierhofer J, Pippan R, Gänser H-P. Modified NASGRO equation for physically short cracks. Int J Fatigue 2014;59:200–7.
[99] Maierhofer J, Gänser H-P, Pippan R. Modified Kitagawa–Takahashi diagram accounting for finite notch depths. Int J Fatigue 2015;70:503–9.
[100] Madia M, Zerbst U. Application of the cyclic r-curve method to notch fatigue analysis. Int J Fatigue 2016;82:71–9.
[101] Yadollahi A, Shamsaei N, Wells DN, Thompson SM, Daniewicz SR. Fatigue behavior and failure analysis of additive manufactured inconel 718 superalloy. Mater Sci Eng A 2016 [submitted for publication].
[102] Murakami Y. Inclusion rating by statistics of extreme values and its application to fatigue strength prediction and quality control of materials. J Res Natl Inst Stand Tehcnol 1994;99:345–51.
[103] Coles S. An introduction to statistical modeling of extreme values. London: Springer; 2001.
[104] Reiss R, Thomas M. Statistical analysis of extreme values. Basel: Birkhauser Verlag; 1997.
[105] ASTM E2283-03. Standard practice for extreme value analysis of nonmetallic inclusions in steels and other microstructural features. American Society for Testing And Materials; 2003.
[106] Maskery I, Aboulkhair NT, Corfield MR, Tuck C, Clare AT, Leach RK, et al. Quantification and characterisation of porosity in selectively laser melted Al-Si10-Mg using X-ray computed tomography. Mater Charact 2016;111:193–204. http://dx.doi.org/10.1016/j.matchar.2015.12.001.
[107] Tammas-Williams S, Zhao H, Léonard F, Derguti F, Todd I, Prangnell P. XCT analysis of the influence of melt strategies on defect population in Ti-6Al-4V components manufactured by selective electron beam melting. Mater Charact 2015;102:47–61. http://dx.doi.org/10.1016/j.matchar.2015.02.008.
[108] Romano S, Beretta S, Brandão A, Gumpinger J. Qualification of AM parts: the application of extreme value statistics for volumetric defect analysis. In: 14th European Conference on Spacecraft Structures, Materials and Environmental Testing (ECSSMET), Toulouse; 2016.